THE JOURNAL OF PHYSICAL CHEMISTRY C

ARTICLE

pubs.acs.org/JPCC

Enzymes Immobilized on Superparamagnetic Fe_3O_4@Clays Nanocomposites: Preparation, Characterization, and a New Strategy for the Regeneration of Supports

Guanghui Zhao, Jianzhi Wang, Yanfeng Li,* Xia Chen, and Yaping Liu

State Key Laboratory of Applied Organic Chemistry, Institute of Biochemical Engineering & Environmental Technology, College of Chemistry and Chemical Engineering, Lanzhou University, Lanzhou 730000, P. R. China

Supporting Information

ABSTRACT: We present a simple method to produce superparamagnetic Fe_3O_4@Clays nanocomposites consisting of magnetic iron oxide nanoparticles orderly self-assembled on some restricted positions of nanoclays. The as-prepared Fe_3O_4@Clays have highly ordered structure, large surface area, and high magnetic sensitivity, as verified by transmission electron microscopy (TEM), IR spectroscopy, X-ray diffraction (XRD), nitrogen adsorption−desorption isotherms, and a vibrating sample magnetometer (VSM). Subsequently, the as-prepared Fe_3O_4@Clays treated with (3-aminopropyl)triethoxysilane are used as immobilization material. The conjugation of glucoamylase, hereby chosen as model enzyme, onto the amino-functionalized magnetic nanoparticles by using glutaraldehyde as a coupling reagent is further demonstrated and assessed based on its activity, kinetics, and thermal stability as well as reusability. Inspired by the structural character of enzyme (containing functional residues that are ideal reaction sites for the immobilization of enzymes once more), two novel regenerated strategies of supports are successfully developed to regenerate the carriers at the end of the life of the immobilized glucoamylase. The quality of glucoamylase immobilized on the regenerated supports is also defined by determining of the enzyme activity, kinetics, thermal stability, and reusability. The results indicate that the strategies for the regeneration of supports are viable. The applicability of the regenerated strategies of supports in the current study is relevant for the conjugation of other enzymes beyond glucoamylase. The regenerated strategies also offer an attractive and flexible alternative to regenerate other traditional supports at the end of the life of the immobilized enzyme.

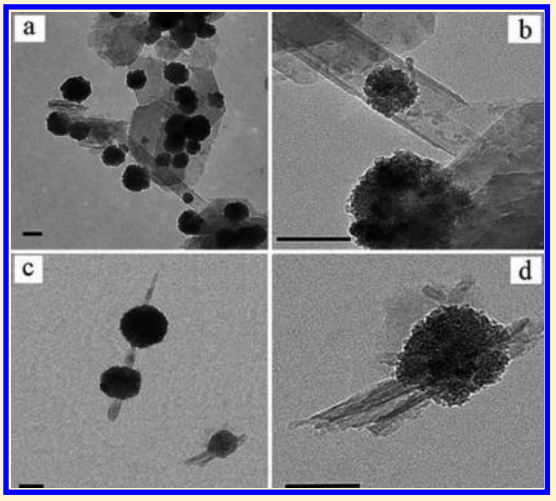

INTRODUCTION

Enzyme immobilization provides a versatile physicochemical tool that allows the reuse or continuous use of enzymes, facilitates substrate and product recovery, prevents product contamination, and, in certain instances, improves the properties of the biocatalyst.[1] However, the industrial applications of the biocatalysts have not yet reached a significant level due to the high cost of enzyme immobilization and the inconvenience in their separation, recycling, and reusing. Therefore, enzyme immobilization is undertaken either for the purpose of basic research or for use in technical processes of commercial interest. Up to now, many different scaffolds and supports with a range of functionality, morphology, and physical properties have been studied for the immobilization of enzymes such as silica,[2−4] polysaccharide,[5] novel aromatic diamine polymers,[6] polymer nanofibers,[7] hydrogels,[8,9] and nanoparticles.[10,11] In recent years, nanostructured materials, such as nanoclays, have attracted considerable interest as an enzyme-immobilization support due to their low-cost, small size, and unusual intercalation properties.[12−15] Another important reason is the presence of silanol groups that, after activation by different functional groups, act as attachment sites for bioactive species.

Clay minerals are layer type aluminosilicates, the most important of which are kaolinite, attapulgite, montmorillonite, beidellite, nontronite, saponite, and hectorite. The structure, chemical composition, exchangeable ion type, and small crystal size of clays are responsible for several unique properties, including a large chemically active surface area, a high cation exchange capacity, interlamellar surfaces having unusual hydration characteristics, and sometimes the ability to modify strongly the flow behavior of liquids. These unique properties make them excellent materials for various applications such as catalysts,[12] templates in organic synthesis,[16] and building blocks for composite materials.[17,18] Moreover, due to their unique physicochemical properties, such as swelling and cation exchange capability (CEC), as well as their

Received: January 6, 2011
Revised: February 28, 2011
Published: March 24, 2011

mechanical and thermal stability, nanoclays also can be efficiently used as matrices for immobilization of biomolecules. Montmorillonite,[12−14,19−21] synthetic beidellite clays,[15] palygorskite, Illite, and kaolinite[21] are examples of nanoclays that enzymes have been immobilized on. However, the major drawback of these studies is that the supports are very hard to disposal and be separated after catalytic reaction. Magnetism makes possible heterogeneous catalysis by which efficient separation of biocatalysts is made feasible, and in addition the process can be carried out continuously. Therefore, clays modified with magnetic nanoparticles are promising materials for the application of enzymes immobilization. Magnetic iron oxide/clays hybrid materials have been described in the literature, including both magnetite (Fe_3O_4)[22] and maghemite (γ-Fe_2O_3).[23−25]

Nevertheless, according to these reports, magnetic nanoparticles are attached on the clay surface. The silanol groups, acting as attachment sites for immobilization of enzyme after activation by different functional groups, could be covered up. This drawback would hinder the further immobilization of enzyme on clays-based nanosupports. Furthermore, these magnetic nanoparticles have very low magnetic sensitivity, which also limits their application.

In the present work, we describe a novel method for the synthesis of magnetic clay composites consisting of magnetic iron oxide nanoparticles orderly self-assembled on some restricted positions of nanoclays. The main novelty of our Fe_3O_4@Clays nanocomposites, compared with the previous reports, mainly includes the following points: (1) modification of clays in restricted positions can alleviate the negative effect on their characteristics from the foreign material, and (2) the high magnetic sensitivity of our Fe_3O_4@Clays nanocomposites makes the separation of clays easy.

The other aim of this paper is to develop a new strategy for the regeneration of supports. In general, reversible enzyme immobilization may be a good option because it allows the reuse of the supports (e.g., expensive materials having excellent mechanical and hydrodynamic properties) and the subsequent reduction of industrial wastes. A number of methods for reversible immobilization of enzymes have been reported, e.g., thiol-disulfide exchange of proteins containing surface thiol groups,[26,27] immobilized metal chelate supports,[28,29] and ionic exchange resins.[30−34] However, all these reversible supports of enzyme immobilization have the drawback of a small surface area or a small immobilization capacity, which limits their application. Moreover, the preparation of these supports requires several steps and special chemicals and procedures. Herein, we propose two novel and facile strategies for the regeneration of general support. The main novelty of the strategies is that the method allows for the regeneration of covalent binding support after inactivation of immobilized enzyme.

In the current work, a model enzyme, glucoamylase, is covalently bounding to our superparamagnetic Fe_3O_4@Clays nanocomposites via a bifunctional agent. Subsequently, the supports are regenerated at the end of the life of the enzyme. The inactivated enzyme immobilized on the supports contains functional residues (e.g., NH_2, COOH, SH, and imidazole groups) that are ideal reaction sites for the immobilization of enzymes once more. Based on these findings, we hypothesize that the spent supports with inactivated enzymes may be regenerated with glutaraldehyde and Cu^{2+}, respectively. After glucoamylase immobilized on the regeneration of supports, different glucoamylase derivatives are obtained, and their properties are investigated to evaluate this hypothesis. It is also important to note that the regeneration strategies developed are not limited to glucoamylase immobilization but are applicable for the conjugation of other proteins.

EXPERIMENTAL SECTION

Enzymes and Reagents. Glucoamylase (exo-1,4-a-D-glucosidase, EC3.2.1.3 from *Aspergillus niger* 10U mg^{-1}) was purchased from Yixing Enzyme Preparation Company (China). Attapulgite nanofibrillar clay with the average diameter of 47 μm was provided by Anhui Mingmei MinChem Co. Ltd. (China). The kaolinite used in this study was provided by China-Kaolinite Company (China) with a diameter of 5−10 μm. All other chemicals were of analytical grade and used as received.

Pretreatment of Clays. The nanoclays were activated with ultrasonication for 1 h in 2 M HCl solution at 30 °C, in order to remove the residual carbon and sodium ions on the clays surface. After exhaustive, nanoclays were then separated by gravity sedimentation followed by several cycles of washing with distilled water until the pH value of the supernatant reached neutral, and the activated nanoclays were dried for 24 h at 80 °C under vacuum. The sample was then desiccated and ground in an agate mortar and finally allowed to filter through a 47 μm sieve before use.

Synthesis of Superparamagnetic Fe_3O_4@Clays Nanocomposites. In a typical procedure, the synthesis of Fe_3O_4 nanoparticles was carried out by modified reduction reactions between $FeCl_3$ and ethylene glycol in the solvothermal system described in the literature.[35] First, NaAc was added for electrostatic stabilization to prevent particle agglomeration. In this system, NaAc was even more important, as its addition seems to assist in the ethylene glycol mediated reduction of $FeCl_3$ to Fe_3O_4. Second, polyethylene glycol was added as a surfactant and as an additional preventative measure against particle agglomeration. The third feature is the increased reaction temperature of 200 °C, which is necessary for the production of Fe_3O_4. The experimental details about the synthesis of the nanocomposites were as follows:[35] 1 g $FeCl_3 \cdot 6H_2O$ was dissolved in 30 mL of ethylene glycol to form a clear solution. Then, 2.7 g of sodiumacetate (NaAc) and 0.75 g of polyethylene glycol were added with constant stirring for 30 min. After that, nanoclays (0.3 g) activated with hydrochloric acid were ultrasonically dispersed in the resulting dispersion for 3 h. The mixture was sealed in a Teflon-lined stainless steel autoclave (50 mL capacity) and maintained at 200 °C for 8 h. Then, the mixture was cooled to ambient temperature. The obtained black magnetite particles were washed with ethanol and deionized water in sequence and dried in vacuum at 60 °C for 24 h.

Amino-Modification of Superparamagnetic Fe_3O_4@Clays Nanocomposites. To modify the final composite nanoparticles with amino groups, 1.0 g of Fe_3O_4@Clays nanocomposites was immersed in 60 mL of xylene for 3 h followed by addition of 6 g of 3-aminopropyltriethoxysilane (APTS) to the mixture. The coupling reaction was carried out at 120 °C by reflux for 12 h. After the reaction, the prepared sample was collected using a magnet, washed with ethanol for three times, and was dried at 60 °C for 24 h under vacuum. The obtained product was denoted as Fe_3O_4@-Clays-NH_2.

Enzyme Immobilization. Glucoamylase was immobilized onto the Fe_3O_4@Clays-NH_2 by a typical glutaraldehyde (GA) activation procedure, where glutaraldehyde was used as a spacer. An appropriate amount of the Fe_3O_4@Clays-NH_2 was submerged into a GA solution composed of 50% GA water solution and deionized water (10%, v/v) and shook for 8 h at room temperature. The activated support was taken out by magnetic

separation, washed several times with deionized water to remove excess GA, and then washed with acetate buffer solution (50 mM, pH 5.5). The obtained product was denoted as Fe_3O_4@Clays-GA. The immobilization process was carried out at 30 °C in a shaking air bath for 8 h. After this, the immobilized glucoamylase was recovered by magnetic separation and thoroughly rinsed with acetate buffer solution (50 mM, pH 5.5) two times to remove unbound glucoamylase. The washed solution was collected to assay the amount of residual enzyme. The resulting immobilized glucoamylase was stored at 4 °C prior to use.

The amount of protein in the enzyme solution and in the washed solution was determined by the Bradford method using bovine serum albumin as a standard,[36] and the amount of protein bound on the carriers was calculated from the formula

$$\text{protein bound(mg/g)} = \frac{(C_i\text{-}C_f)V}{W} \quad (1)$$

where protein bound is the amount of bound enzyme onto Fe_3O_4@Clays nanocomposites (mg g^{-1}), C_i and C_f are the concentrations of the enzyme protein initial and final in the reaction medium (mg mL^{-1}), V is the volume of the reaction medium (mL), and W is the weight of the carriers (g). All data used in this formula are the average of triplicate experiments.

The Regeneration of Supports for Enzyme Repeated Immobilization. The supports are regenerated at the end of the life of the immobilized glucoamylase by a glutaraldehyde or Cu^{2+} activation procedure. The inactivated enzyme immobilized on the Fe_3O_4@Clays nanocomposites contains functional residues (e.g., NH_2, COOH, SH, and imidazole groups) that are ideal reaction sites for the immobilization of enzymes once more. Therefore, the glutaraldehyde activation procedure is as follows: an appropriate amount of the inactivated enzyme immobilized on the Fe_3O_4@Clays was thoroughly inactivated with acetone/ethanol (1/1, V/V) under the condition of ultrasonication for 1 h and subsequently high temperature (100 °C) for 30 min and then rinsed with acetate buffer solution (50 mM, pH 5.5). After this, the pretreated supports were submerged into a GA solution composed of 50% GA water solution and deionized water (10%, v/v) and shaken gently for 8 h at room temperature. Cu^{2+} activation procedure is as follows: Cu(II) ion was chelated with the functional groups of the inactivated enzyme immobilized on the Fe_3O_4@Clays nanocomposites. A 5 mg mL^{-1} solution of Cu(II) ions was prepared from sulfate salts in distilled water. The inactivated enzyme immobilized on Fe_3O_4@Clays was suspended in the Cu(II) ions solution at room temperature for 6 h.

The regenerated supports were taken out, washed several times with acetate buffer solution (50 mM, pH 5.5), and submerged into 5.0 mL of glucoamylase buffer solution (pH 5.5, 50 mM acetate buffer including 0.6 mg of glucoamylase). The repeated immobilization process was carried out at 30 °C in a shaking air bath for 8 h. Finally, the regenerated supports were taken out and thoroughly rinsed with acetate buffer (50 mM, pH 5.5). The amount of immobilized protein on the regenerated supports was determined as described above.

Enzyme Activity. The reaction rate of the free and immobilized glucoamylase preparations was determined according to the method reported by Nelson et al.[37] with only minor modification. In the standard conditions, soluble starch was used as the substrate, which composed of 0.5 mL of 10 wt.% soluble starch gelatinized in water and 2.5 mL acetate buffer solution (50 mM, pH 5.5). The reaction was started by the addition of 0.5 mL of free glucoamylase (0.236 mg mL^{-1}) or 0.1 g of immobilized glucoamylase. The mixture was incubated at 55 °C under reciprocal agitation at 120 strokes per minute. After 15 min of reaction, agitation was stopped, and then the reaction was terminated by adding 5 mL of NaOH solution (0.1 M). The glucose content was determined using the DNS method.[38] The amount of glucose was obtained from the calibration curve and used in the calculation of enzyme activity. All activity measurement experiments were carried out three times, and the relative standard deviation is less than 1.0%. One unit of glucoamylase activity is defined as the amount of enzyme that produces 1.0 mmol of glucose from dissolubility starch per minute under the assay conditions. The relative activity (%) was the ratio between the activity of every sample and the maximum activity of sample. The activity recovery (%) was the ratio between the activity of immobilized glucoamylase and the activity of free glucoamylase. All experiments of activity measurement were carried out at least three times, and the experimental error was less than 3%.

Determination of the Kinetic Constants. The Michaelis constant (K_m) and the maximum reaction velocity (V_{max}) of the free and immobilized glucoamylase were determined by measuring initial rates of the reaction in acetate buffer solution (50 mM, pH 5.5) at 55 °C. The apparent kinetic constants of the immobilized glucoamylase or free glucoamylase were determined by measuring initial rates of the reaction with soluble starch [0.5−3.5% (w/v)] in acetate buffer (50 mM, pH 5.5) at 55 °C. For this purpose, equivalent free or immobilized glucoamylase was added to soluble starch solution of different concentrations, and the initial activities were determined as above-described. K_m and V_{max} values were calculated from initial reaction rate using the Lineweaver−Burk plots through the Michaelis−Menten kinetic equations. V_{max} was proportional to the enzyme concentration, [E], as given in the following equation: $V_{max} = K_{cat}[E]$, where K_{cat} was an apparent rate constant having a unit of reciprocal time (s^{-1}). This K_{cat} encompassed the chemical transformation events leading to product formation from the ternary enzyme conformation.[39]

Characterization. Powder X-ray diffraction (XRD, Rigaku D/MAX-2400 X-ray diffractometer with Ni-filtered Cu Kα radiation) was used to investigate the crystal structure of the magnetic nanoparticles. FT-IR spectra were obtained in transmission mode on a Fourier-transform infrared spectrophotometer (American Nicolet Corp. Model 170-SX) using the KBr pellet technique.[40] Transmission electron microscopy (TEM, FEI Tecnai G20) images were obtained to elucidate the dimensions and the structural details of the nanoparticles. TEM specimens were made by placing a drop of the nanoparticle suspension on a carbon-coated copper grid. The N_2 adsorption/desorption isotherm was measured at liquid nitrogen temperature (77 K) using a Micromeritics ASAP 2010 M instrument. The specific surface area was calculated by the Brunauer−Emmett−Teller (BET) method. The pore size distribution was obtained from the Barret−Joner−Halenda (BJH) method. Magnetization measurements were performed on a vibrating sample magnetometry (VSM, LAKESHORE-7304, USA) at room temperature. Scanning electron microscopy (SEM, JSM-6380Lv, JEOL, Japan; and JSM-6701F, JEOL, Japan) images were obtained to elucidate the dimensions and the structural details of the nanoparticles.

RESULTS AND DISCUSSION

Fabrication of Nanostructured Fe_3O_4@Clays and Nanocomposites Morphology. The chemical process to fabricate the material is thoroughly described in the Experimental Section, and

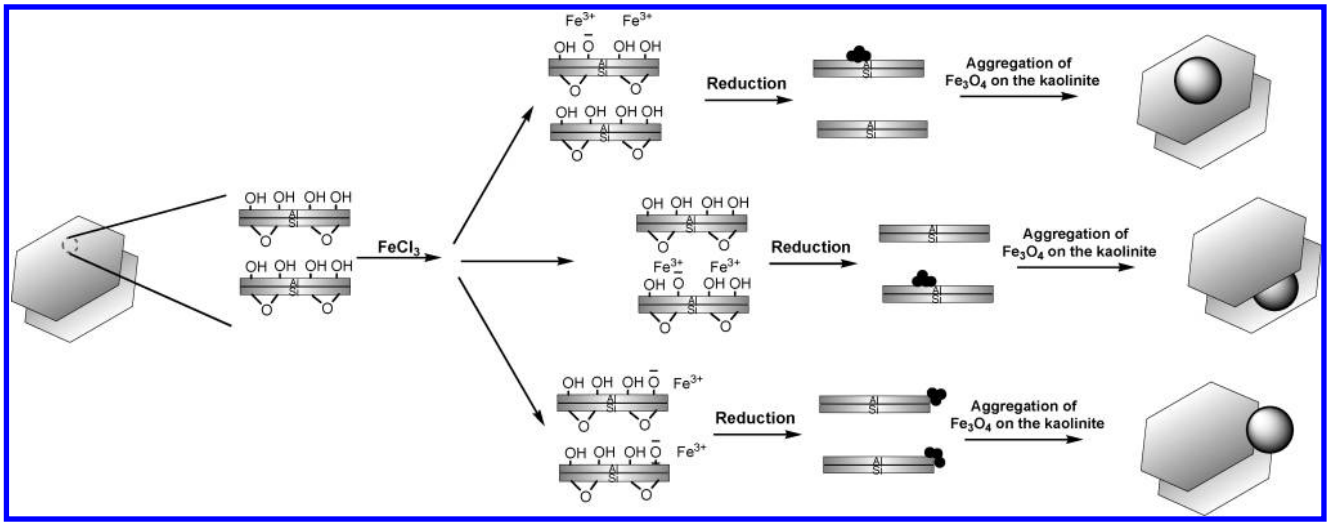

Figure 1. Schematic illustration of the synthesis process used to produce a new class of Fe_3O_4@Kaolinite nanocomposites.

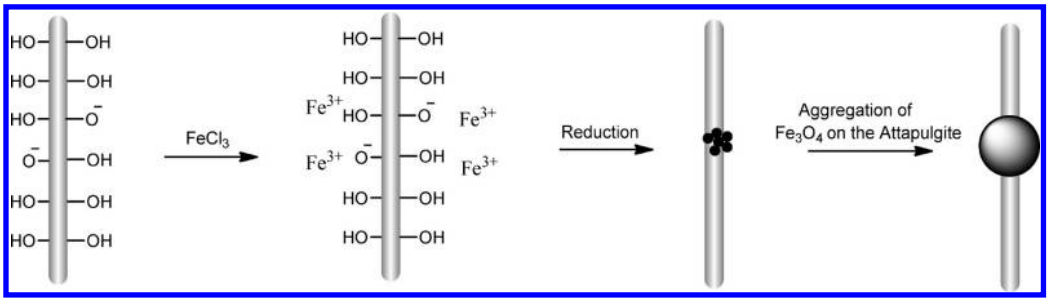

Figure 2. Schematic illustration of the synthesis process used to produce a new class of Fe_3O_4@ATP nanocomposites.

it is visually summarized schematically in Figure 1 and Figure 2. Kaolinite, $Si_2Al_2O_5(OH)_4$, is a 1:1 phyllosilicate made up of one tetrahedral sheet linked tone octahedral sheet. Each layer contains a sheet of SiO_4 tetrahedra forming six-membered silicate rings connected to the sheet of AlO_6 octahedra through the apical oxygens.[41] The layers are held together via hydrogen bonds, dipolar interactions, and attractive van der Waals forces.[42] Attapulgite (ATP, so-called palygorskite) is a kind of hydrated octahedral layered magnesium aluminum silicate clays present in nature as a fabrillar silicate clay mineral with a length of 500−2000 nm and diameter of 10−25 nm. ATP and Kaolinite have permanent negative charges and exchangeable cations on their surface, which enable them to be modified by positive metal ions, to serve as nucleation precursors. In our system, iron(III) cations in the solution would like to attach to some particular positions of the Kaolinite (or ATP) with high density of negative charges or exchangeable cations and then in situ reduced into very fine magnetite particles during following hydrothermal treatment.[43] These tiny particles have much high surface energy and are preferentially attached onto the surface of clays from polyol solution automatically. The tiny nanoparticles will then serve as the nuclei for the growth of magnetite nanoparticles.[44]

Figure 3 shows typical transmission electron microscopy (TEM) images of as-synthesized Fe_3O_4@Clays nanocomposites. TEM images (Figure 3a,b) confirm the different location of Fe_3O_4 nanoparticles with an average particle size of 150 nm around Kaolinite with a typical sheet-like structure. It can be observed that there are three different derivatives in the microstructure of the

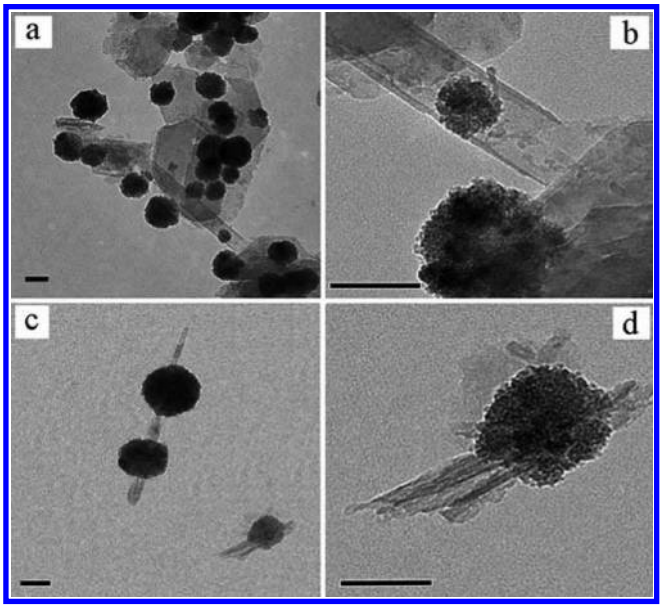

Figure 3. TEM images of Fe_3O_4@Kaolinite nanocomposites (a, b) and Fe_3O_4@ATP nanocomposites (c, d). Scale bars: 100 nm.

as-synthesized Fe_3O_4@Kaolinite nanocomposites (Figure 1 and Figure 3a,b): Fe_3O_4 nanoparticles can be anchored on the external surfaces and the edges of the clay sheets or intercalated within

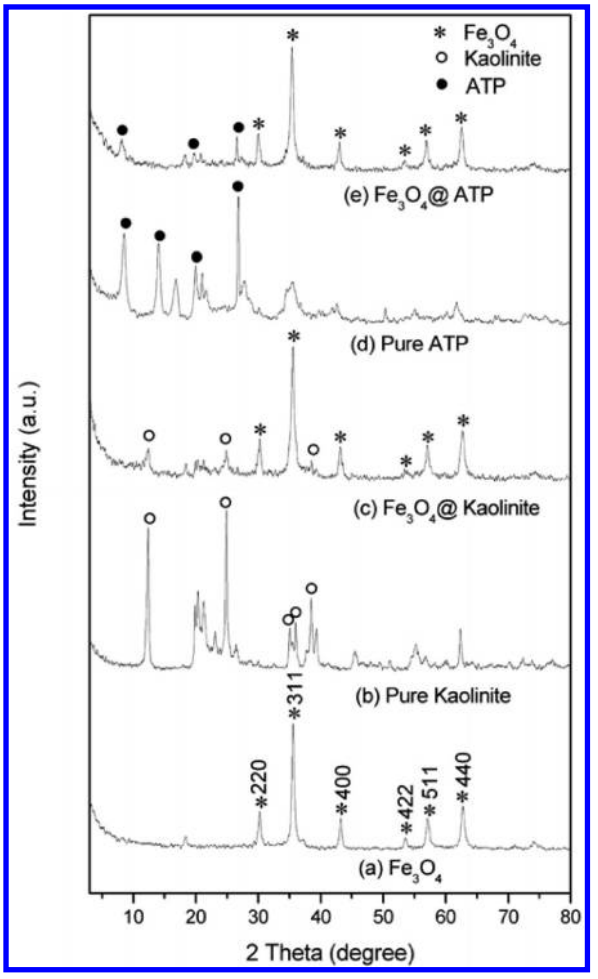

Figure 4. Wide-angle XRD patterns of (a) Fe_3O_4 particles, (b) Pure Kaolinite, (c) Fe_3O_4@ Kaolinite, (d) Pure ATP, and (e) Fe_3O_4@ ATP.

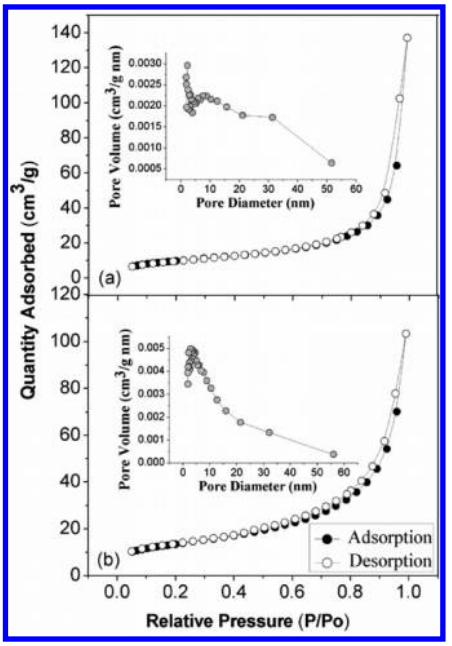

Figure 5. N_2 adsorption/desorption isotherms of (a) Fe_3O_4@Kaolinite and (b) Fe_3O_4@ATP nanocomposites. The inset shows the pore size distribution curve obtained from the adsorption data.

interlayer space. (1) In our system, iron(III) cations in the solution could attach to the external sites of Kaolinite, which leads to the location of Fe_3O_4 nanoparticles with an average particle size of 180 nm on the external surface of Kaolinite (Figure 1 and Figure 3a). The nanocomposites with this microstructure were denoted as outer-sphere Fe_3O_4@Kaolinite nanocomposites. (2) Iron(III) cations in the solution could be intercalated into the interlayer space of Kaolinite by electrostatic forces or ionic exchange, which leads to the formation of inner-sphere Fe_3O_4@Kaolinite nanocomposites (Figure 1 and Figure 3b). A very small feature of Fe_3O_4 nanoparticles with an average particle size of 50 nm in this microstructure suggests that the nanoparticles are embedded between the aluminosilicate layers, and the growth of Fe_3O_4 nanoparticles is prevented by the aluminosilicate layers. (3) In Kaolinite, Al and Si atoms exposed to the crystallite edges are partially hydrolyzed to silanol (SiOH) and aluminol (AlOH) groups. These unsaturated edge sites are much more reactive than the saturated basal sites. Therefore, iron(III) cations in the solution could also be anchored on the edge sites, which results in marginal-sphere Fe_3O_4@Kaolinite nanocomposites (Figure 1 and Figure 3b). The size and morphology of the as-synthesized Fe_3O_4@ATP nanocomposites (Figure 3c,d) were also investigated by transmission electron microscopy (TEM). As shown in Figure 3c,d, the TEM investigation clearly indicates that the ATP needles pass through the middle of Fe_3O_4 nanoparticles with an average particle size of 150 nm. For the synthesis reaction, its possible mechanism is shown in Figure 2: There are negative charges and −OH groups at the surface of the ATP needles. First, iron(III) cations in the solution also could be anchored on the surface by nonspecific adsorption (cation exchange), or specific adsorption, which is based upon adsorption reactions at −OH groups at the ATP surfaces and edges and which is characterized by more selective and less reversible reactions. Subsequently, iron(III) cations anchored on the surface in situ reduced into very fine magnetite particles during following hydrothermal treatment, these tiny Fe_3O_4 aggregated around the ATP templates in some positions and formed spherical aggregation.

The crystal structure of the as-synthesized Fe_3O_4@Clays nanocomposites and pure clays was investigated using X-ray diffraction (XRD) and is shown in Figure 4. In Curves c and e: the characteristic diffraction peaks of magnetite (Fe_3O_4) are present in both as-synthesized Fe_3O_4@Clays nanocomposites, which can be assigned to the (220), (311), (400), (422), (511), and (440) planes according to JCPDS 19-629 (JCPDS = Joint Committee on Powder Diffraction Standards). Moreover, Curves c and e, apart from the Fe_3O_4 reflections, present some additional peaks that obviously originate from corresponding clays (Curves b and d), and no obvious peaks from other phases were observed. The analysis result indicates that the crystal structure of as-synthesized Fe_3O_4@Clays nanocomposites comprises two phases of cubic Fe_3O_4 and corresponding clays. For the nanocomposite (Curves c and e), the diffractive peaks of Fe_3O_4 appear broader suggesting smaller particle size (ca. 8.4 nm for pure iron oxide and ca. 4.6 nm for the composite, estimated by Scherrer's equation considering only the presence of the maghemite phase).

The N_2 adsorption/desorption isotherm of as-synthesized Fe_3O_4@Clays nanocomposites exhibits typical IV-type isotherms with H_3-hysteresis loops (Figure 5), which indicates the presence of textual mesopores. We ascribe the soft slope for relative pressures, P/P_0, between 0.1 and 0.9 to the external area of the particles, and the high volume uptake at $P/P_0 > 0.9$ to the meso- and

dx.doi.org/10.1021/jp200156j |J. Phys. Chem. C 2011, 115, 6350–6359

Table 1. Physical Properties of Fe_3O_4@Clays Nanocomposites[a]

sample	S_{BET} (m^2/g)	V_P (cm^3 g^{-1})	average pore width (nm)	NH_2 amount (mmol g^{-1})	M_S (emu g^{-1})
Fe_3O_4@ Kaolinite	36.2	0.21	22.06	0.51	38.56
Fe_3O_4@ATP	48.5	0.16	13.17	1.22	40.85

[a] S_{BET}: Brunauer−Emmett−Teller surface area; V_P: BJH desorption cumulative volume of pores; M_S: saturation magnetization.

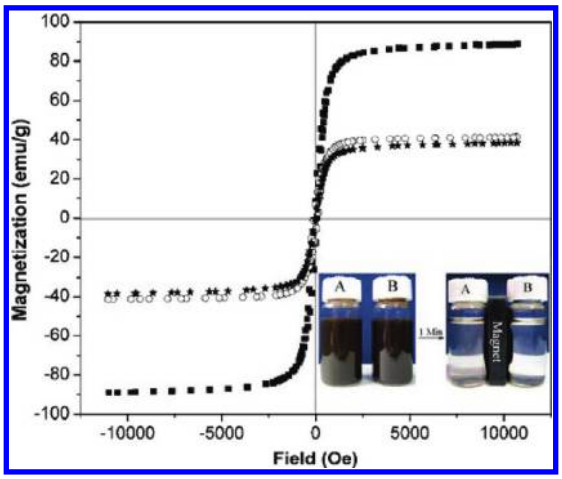

Figure 6. The magnetic hysteresis loops of pure Fe_3O_4 (■), Fe_3O_4@-Kaolinite nanocomposites (★), and Fe_3O_4@ATP nanocomposites (○). The inset shows the photograph of Fe_3O_4@clays nanocomposites (A: Fe_3O_4@Kaolinite nanocomposites; B: Fe_3O_4@Kaolinite nanocomposites) dispersion in water (left) and their magnetic response placed in external magnetic field (right).

macropores formed by the interparticular space.[45] The hysteresis loops appeared nearly $p/p_0 = 0.8$, indicating that the pore size was relative large. This is confirmed by the pore size distribution curve (inset Figure 5), and the average pore diameters of 22.06 nm for Fe_3O_4@Kaolinite and 13.17 nm for Fe_3O_4@ATP are a good match for the dimensions of glucoamylase molecules. The pore sizes of Fe_3O_4@Kaolinite were in a very wide range, indicating bimodal porosity in the mesoporous and macroporous regimes for Fe_3O_4@-Kaolinite. This type of porosity would provide an efficient transport pathway for reactants to the interior of the Fe_3O_4@Clays, which is beneficial for catalytic properties.[46] The Brunauer−Emmett−Teller (BET) surface area of Fe_3O_4@Kaolinite nanocomposites has been calculated to be 36.2 m^2 g^{-1}, which is less than that of Fe_3O_4@ATP nanocomposites (48.5 m^2 g^{-1}). Meanwhile, it is interesting to note that Fe_3O_4@Kaolinite nanocomposites showed much higher average pore diameter and micropore volume compared to Fe_3O_4@ATP nanocomposites (Table 1). As we all know, the parameter of pore diameter and micropore volume is more important for enzyme immobilization than that of surface area, thus we hypothesize that Fe_3O_4@Kaolinite nanocomposites are more available for enzyme immobilization.

Magnetic Properties of Fe_3O_4@Clays Nanocomposites. The magnetic behavior of the as-synthesized pure Fe_3O_4 and as-synthesized Fe_3O_4@Clays nanocomposites were studied using a vibrating sample magnetometer (VSM) at room temperature. The field-dependent magnetization curves in Figure 6 show that negligible hysteresis loops were observed, indicating the characteristic superparamagnetic behavior of all the nanoparticles at room temperature. From Figure 6, it can be seen that the saturation magnetization of pure Fe_3O_4 nanoparticles was found to be 88.97 emu g^{-1}. However, owing to the existence of clays, the saturation magnetization of Fe_3O_4@Clays nanocomposites decreases to 38.56 emu g^{-1} for Fe_3O_4@Kaolinite and 40.85 emu g^{-1} for Fe_3O_4@ATP compared to pure Fe_3O_4 nanoparticles, which is basically consistent with the mass ratio of Fe_3O_4 content in the nanocomposites. As shown in the inset of Figure 6, the Fe_3O_4@Clays nanocomposites show fast response (1 min) to the external magnetic field because of their high magnetization, which suggests this level of saturation magnetization is deemed sufficient for the applications of enzyme immobilization.

Immobilization of Glucoamylase onto Fe_3O_4@Clays. The immobilization of glucoamylase onto the Fe_3O_4@Clays is shown schematically in Figure 7, and which describes the basic strategy for the regeneration of supports. Like most clays and oxide surfaces, the abundant surface hydroxyl groups (−OH) present on the Fe_3O_4@Clays nanocomposites are the basis for their surface modifications. In the current study, conventional alcohol-based silanization protocol with APTS resulted in 0.51 mmol g^{-1} for Fe_3O_4@Kaolinite and 1.22 mmol g^{-1} for Fe_3O_4@ATP accessible amine group on the particle surface when elemental analysis (C, H, and N) was performed by Vario EL element analyzer. The amine group density is accorded with the Brunauer−Emmett−Teller (BET) surface area of Fe_3O_4@Clays nanocomposites. Upon silanization, the existence of amine group is more convincingly represented by the C−N, N−H signal (~1319 cm^{-1} and ~1566 cm^{-1}) from the corresponding IR spectra (Figure 8). Glutaraldehyde could react with amino, thiol, phenol, and imidazole groups of proteins.[47] Hence, Fe_3O_4@-Clays-GA having aldehyde groups is an excellent carrier for immobilization of enzymes. Immobilization procedure is quite simple and involves the reaction of Fe_3O_4@Clays-GA with aqueous glucoamylase solution at room temperature. The amounts of bound protein are 9.13 mg g^{-1} on the Fe_3O_4@Kaolinite nanocomposites and 6.24 mg g^{-1} on the Fe_3O_4@ATP nanocomposites. Interestingly, compared to that on the Fe_3O_4@ATP nanocomposites, there is a significant increase of the amount of bound protein on the Fe_3O_4@-Kaolinite nanocomposites. This result can be explained by the fact that the remarkable high average pore diameter and micropore volume of the Fe_3O_4@Kaolinite nanocomposites can provide more available pores for the covalent coupling of glucoamylase. Although the surface area of Fe_3O_4@ATP nanocomposites is higher than those of Fe_3O_4@Kaolinite nanocomposites, most of them belong to micropore, which may not contribute to immobilization of glucoamylase. This is confirmed by the pore size distribution curve of Fe_3O_4@ATP nanocomposites (inset Figure 5b), and most of the micropore diameter are too narrow, and glucoamylase molecules cannot be immobilized in these micropore.

The Regeneration of Supports. For immobilized enzyme, one of the most important advantages is reuse stability, which can effectively reduce the cost in industry applications. To evaluate the reuse stability, the glucoamylase-immobilized Fe_3O_4@Clays nanocomposites were washed with acetate buffer (50 mM, pH 5.5) after any run and reintroduced into a fresh solution. This process was repeated up to 10 cycles. The variation of activity of the

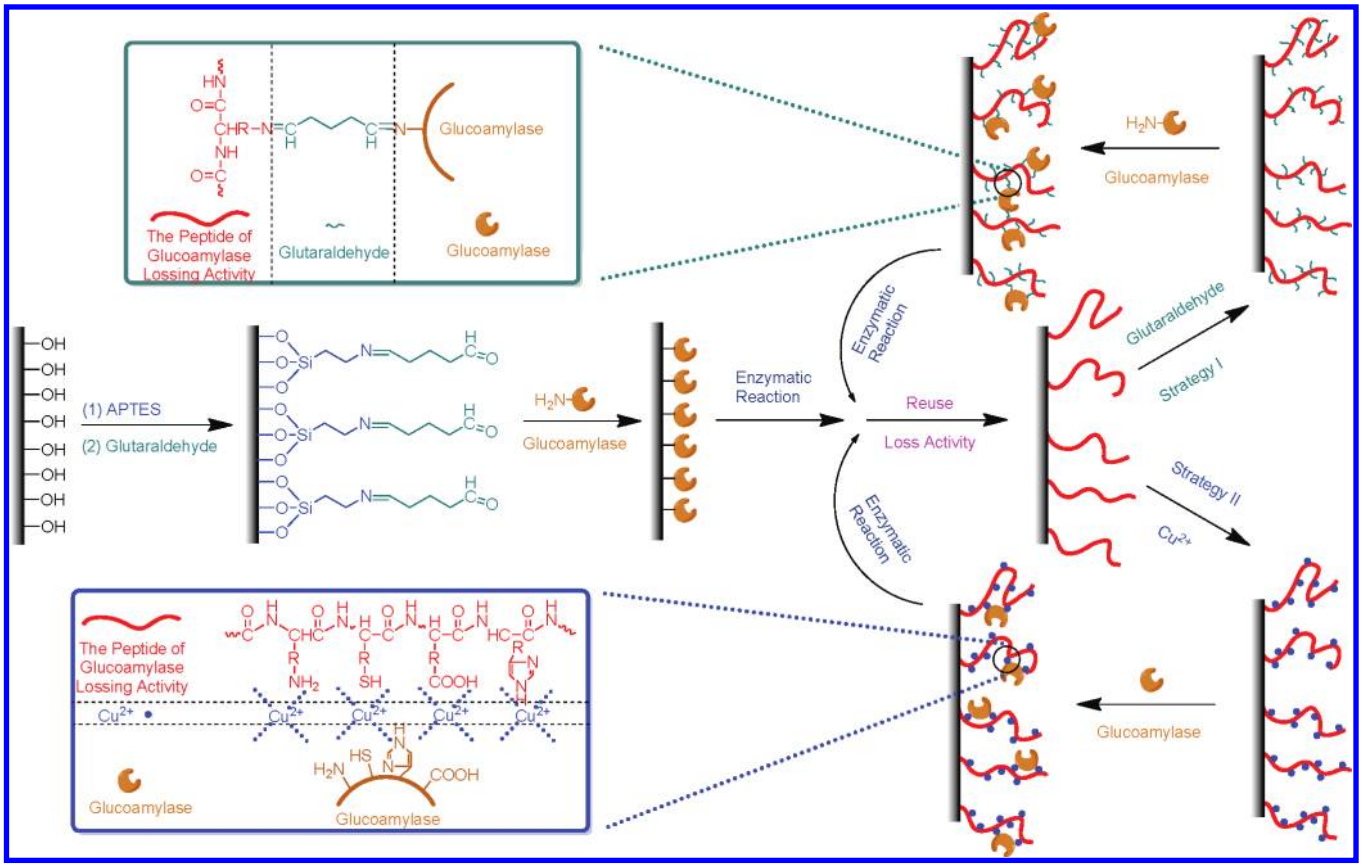

Figure 7. Schematic illustration of glucoamylase immobilized onto the Fe_3O_4@Clays and the basic strategy for the regeneration of supports.

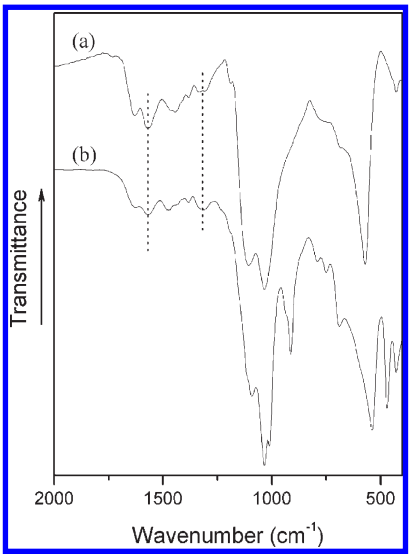

Figure 8. The IR spectra of Fe_3O_4@ATP-NH_2 (a) and Fe_3O_4@Kaolinite-NH_2 (b).

immobilized glucoamylase after multiple reuses is showed in Figure 10. It was observed that the residual activity of the immobilized enzymes is 71.86% for the Fe_3O_4@Kaolinite and 64.96% for the Fe_3O_4@ATP after the 10th reuse, indicating that the Fe_3O_4@Kaolinite carriers offered a more stable covalent linkage toward glucoamylase than the Fe_3O_4@ATP support. The immobilized enzyme also could lose its activity completely after several times of reuse. Therefore, the regeneration of supports at the end of the life of the immobilized enzyme, which can effectively reduce the cost in industry applications, is very essential. The most general, easiest to perform, and oldest protocol for reversible immobilization of enzymes (with an easy regeneration of the support) is the adsorption of enzymes on ionic exchange resins (mainly on anionic exchange supports). However, the adsorption is not generally very strong. Some of the adsorbed proteins will desorb during washing and operation. Moreover, the preparation of these supports requires several steps and special chemicals and procedures. Herein, we propose two novel and facile strategies for the regeneration of supports. The method allows for the reusability of covalent binding support after inactivation of immobilized enzyme. The regeneration of supports in the report is carried out in three steps; first, immobilized enzymes are heated to denature the proteins to expose functional residues (e.g., NH_2, COOH, SH, and imidazole groups) of immobilized enzyme to the solvent, which make it easier for glutardialdehyde (or Cu^{2+}) to activate the supports. As the temperature is increased, a number of bonds in the protein molecule are weakened. The first affected are the long-range interactions that are necessary for the presence of tertiary structure. As these bonds are first weakened and are broken, the protein obtains a more flexible structure and the groups are exposed to solvent. If heating ceases at this stage the protein should be able to readily refold to the native structure. As heating continues, some of the cooperative hydrogen bonds that stabilize helical structure will begin to break. As these bonds are broken, water can interact with and form new hydrogen bonds with the amide nitrogen and carbonyl oxygens of the peptide bonds. The presence of water further weakens nearby hydrogen bonds by causing an increase in

Table 2. Activity and Kinetic Parameters of the Free and Immobilized Glucoamylase[f]

biocatalysts	protein loading (mg g^{-1})	specific activity (mmol mg^{-1} h^{-1})[d]	relative activity (%)[e]	K_m (mM)	K_{cat} ($\times 10^3$ s^{-1})	K_{cat}/K_m ($\times 10^3$ mM^{-1} s^{-1})
free enzyme	-	4.25	100	0.22	1.39	6.32
Fe_3O_4@Kaolinite[a]	9.13	2.52	59.29	0.82	2.42	2.95
$R1_{Kaolinite}$-GA[b]	4.06	2.56	60.24	0.81	2.35	2.90
$R1_{Kaolinite}$-Cu^{2+}[c]	4.21	2.83	60.00	0.63	1.72	2.73
Fe_3O_4@ATP	6.24	2.33	54.82	0.92	2.73	2.97
$R1_{ATP}$-GA	3.39	2.36	55.53	0.93	2.82	3.03
$R1_{ATP}$-Cu^{2+}	3.51	2.41	56.71	0.85	2.37	2.79

[a] Glucoamylase immobilization was carried out in the buffer solution of pH 5.5. [b] The spent Fe_3O_4@Kaolinite support with inactivated enzymes was regenerated with glutaraldehyde at the first time. [c] The spent Fe_3O_4@Kaolinite support with inactivated enzymes was regenerated with Cu^{2+} at the first time. [d] Calculated using the conversion data obtained at 15 min, expressed as mmol of glucose reacted per milligram of protein per hour. [e] Relative activity based on that of free enzyme. [f] K_m: Michaelis constant; K_{cat}: turnover number; K_{cat}/K_m: enzyme efficiency.

the effective dielectric constant near them.[48] As the helical structure is broken, functional groups are exposed to the solvent. Subsequently, the support is activated with a bifunctional linker (glutaraldehyde) or Cu^{2+}, and finally immobilization of the enzyme in a usual procedure is carried out (Figure 7). There was a sharp decrease in the immobilization capacities of the regenerated supports comparing to the original one (Table 2). However, the immobilization capacities of the regenerated supports did not significantly change during the following three regeneration cycles (see the Supporting Information). Several speculate could be used to explain this phenomenon. On the one hand, loss of Fe_3O_4@Clays nanocomposites to the repeated usage and multiple handling procedures of the regeneration reduced the amount of biocatalyst present, which has a significant impact for the immobilization capacities of the regenerated supports. On the other hand, glucoamylase molecules were reserved on the Fe_3O_4@Clays as the new reaction sites for the immobilization of glucoamylase molecules once more. However, the glucoamylase molecules could not be immobilized in the micropores which only allow the immobilization of glucoamylase at the first time because of the small pore diameter and volume.

Catalytic Property of Immobilized Glucoamylase. The catalytic property of the glucoamylase immobilized on Fe_3O_4@Clays nanocomposites and the regenerated supports was investigated using starch as the substrate, and the results are presented in Table 2. As shown in Table 2, in comparison with the free enzyme, the immobilized glucoamylase under its optimum reaction condition retains 59.29% of the activity on the Fe_3O_4@Kaolinite and 54.82% on the Fe_3O_4@ATP. Moreover, it can be observed that the regenerated supports showed a similar specific activity toward the original one, suggesting that the new strategies for the regeneration of supports were effective in maintaining high expression of glucoamylase activity.

The catalytic activities of the glucoamylase immobilized on Fe_3O_4@Clays nanocomposites and the regenerated supports were further characterized by turnover number (K_{cat}) and enzyme efficiency (K_{cat}/K_m). K_m and K_{cat} values were obtained according to the Lineweaver−Burk equation as described in the Experimental Section. The values of the kinetic parameters K_m and K_{cat} are summarized in Table 2. The glucoamylase immobilized on Fe_3O_4@Clays nanocomposites and the regenerated supports exhibit a higher value of Michaelis constant K_m than free glucoamylase, reflecting higher apparent affinity of the substrate to the free glucoamylase. The similar K_m values for the glucoamylase immobilized on Fe_3O_4@Clays nanocomposites and the regenerated supports indicated that they all have a similar affinity to the substrate. However, K_{cat}/K_m values of the glucoamylase immobilized

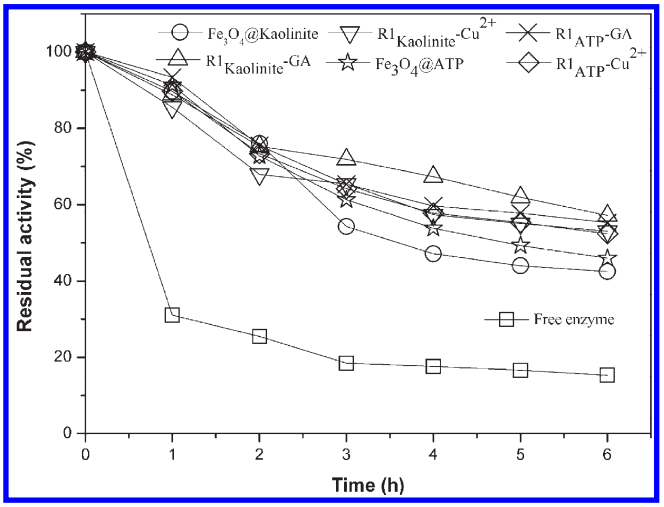

Figure 9. Thermal stabilities of glucoamylase immobilized on Fe_3O_4@Clays nanocomposites and the regenerated supports in comparison to free glucoamylase.

on Fe_3O_4@Clays nanocomposites and the regenerated supports are lower than those of free glucoamylase, which implies the accessibility to the active sites on the immobilized glucoamylase to some extent was hindered as a result of mass transport and diffusion limitation.[49] Noticeably, the comparable K_{cat}/K_m values for the glucoamylase immobilized on Fe_3O_4@Clays nanocomposites and the regenerated supports confirmed that the regenerated supports does not affect the enzyme efficiency.

Stability and Reusability of Immobilized Glucoamylase. The stability of an enzyme is critical to its practical applications. Figure 9 shows the stability of glucoamylase immobilized on Fe_3O_4@Clays nanocomposites and the regenerated supports over 6 h of testing at 60 °C in acetate buffer solution (50 mM, pH 5.5). Both preparations exhibited a similar trend, whereas the immobilized glucoamylase decreased less and more slowly than the free one. The catalytic activity of glucoamylase immobilized on Fe_3O_4@Clays nanocomposites and the regenerated supports retained their initial activity of about 40−60% after 6 h. In sharp contrast, the free glucoamylase only retained their initial activity of about 15% after 6 h. These results demonstrated that the thermal stability of glucoamylase immobilized on Fe_3O_4@Clays nanocomposites and the regenerated supports was much better than the free one. This could be explained by the carriers enhancing the enzyme rigidity, protected it from unfolding and prevented the

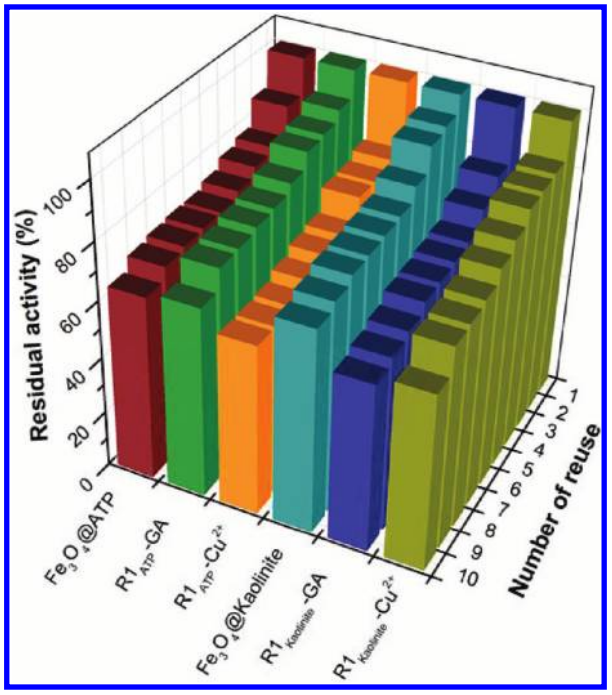

Figure 10. Reuse of glucoamylase immobilized on Fe_3O_4@Clays nanocomposites and the regenerated supports for hydrolyzing starch.

conformation transition of the enzyme at high temperature. These results indicated that the immobilization procedures (glucoamylase immobilized on Fe_3O_4@Clays nanocomposites and the regenerated supports) had considerably improved the thermal stability.

It is important to investigate the performance of immobilized enzymes during recycled use for potential industrial applications. The advantage of the regenerated biocatalyst prepared in this work lies not only in its facile strategy for the regeneration of covalent binding supports but also in its ease of recovery and recycling. Glucoamylases immobilized on Fe_3O_4@Clays nanocomposites and the regenerated supports were recycled for the hydrolyzation of starch. The reaction was performed for 15 min at 55 °C, after which the spent immobilized glucoamylases were recovered by magnetic separation, washed three times with acetate buffer solution (50 mM, pH 5.5), and then used again for a fresh reaction. The assay conditions remained the same as described above. As it can be seen in Figure 10, when ten reaction cycles were completed, the residual activities of glucoamylase immobilized on Fe_3O_4@Clays nanocomposites and the regenerated supports are all approximately 60%. Obviously, the results indicated that the enzyme immobilization onto Fe_3O_4@Clays nanocomposites significantly increases its operational stability. Furthermore, the excellent reusability of glucoamylase immobilized on the regenerated supports further verified that the strategies for the regeneration of supports are viable.

CONCLUSIONS

In this study, a novel kind of superparamagnetic nanocomposites with magnetic iron oxide nanoparticles orderly self-assembled on some restricted positions of nanoclays, i.e. superparamagnetic Fe_3O_4@Clays nanocomposites, was successfully prepared by a facile solvothermal process. The method employed may provide a way for fabricating new classes of magnetic nanocomposites with high magnetic sensitivity and highly ordered structure. Because of their useful magnetic properties and unique porosities, the Fe_3O_4@Clays nanocomposites would have great potential for application as enzyme immobilization, catalysts, targeted drug delivery, adsorbents, and so on. In the current work, the obtained Fe_3O_4@Clays were used as supports for glucoamylase immobilization by covalent coupling. The immobilized glucoamylase exhibited superior thermal stability and reusability. It can be concluded that the superparamagnetic nanocomposite carriers provide an economical, efficient, and selective system for enzyme immobilization. However, the immobilized enzyme also could lose its activity completely after several times of reuse. Therefore, the regeneration of supports at the end of the life of the immobilized enzyme, which can effectively reduce the cost in industry applications, is very essential. We describe a novel, simple, and convenient method for the regeneration of supports: the spent supports with inactivated enzymes were regenerated with glutaraldehyde and Cu^{2+}, respectively. The regenerated biocatalyst reserved its original reusability. Moreover, the glucoamylase immobilized on the regenerated supports exhibited more superior thermal stability comparing to the original one, because the inactive glucoamylase immobilized on spent supports "wrapped" the fresh glucoamylase during regeneration. The results indicated that the strategies for the regeneration of supports were successful and viable. In principle, the strategies employed can regenerate other traditional carriers at the end of the life of the immobilized enzyme, which we will further investigate in the future.

ASSOCIATED CONTENT

Supporting Information. The SEM images of as-synthesized Fe_3O_4@Clays nanocomposites, the comparison of the pore size distribution (PSD) for the pure clays and Fe_3O_4@Clays, and detailed results for repeated regeneration of Fe_3O_4@Clays nanocomposites. This material is available free of charge via the Internet at http://pubs.acs.org.

AUTHOR INFORMATION

Corresponding Author
*E-mail: liyf@lzu.edu.cn.

ACKNOWLEDGMENT

The authors thank the financial support from the National Natural Science Foundation of China (No.21074049), the National Training Fund for Person with Ability of Basic Subjects established by the Natural Science Foundation of China (J0730425), and the Opening Foundation of State Key Laboratory of Applied Organic Chemistry (SKLAOC-2009-35).

REFERENCES

(1) Cao, L. *Curr. Opin. Chem. Biol.* **2005**, *9*, 217–226.
(2) Zhao, D. Y.; Huo, Q. S.; Feng, J. L.; Chmelka, B. F.; Stucky, G. D. *J. Am. Chem. Soc.* **1998**, *120*, 6024–6036.
(3) Schmidt-Winkel, P.; Lukens, W. W.; Zhao, D. Y.; Yang, P. D.; Chmelka, B. F.; Stucky, G. D. *J. Am. Chem. Soc.* **1999**, *121*, 254–255.
(4) Jie, L.; Jie, F.; Yu, C. Z.; Zhang, L. Y.; Jiang, S. Y.; Bo, T.; Zhao, D. Y. *Microporous Mesoporous Mater.* **2004**, *73*, 121–128.
(5) Grunwald, P.; Hansen, K. *Solid State Ionics* **1997**, *101−103*, 863–867.
(6) Li, X. G.; Huang, M. R.; Duan, W. *Chem. Rev.* **2002**, *102*, 2925–3030.
(7) Jia, H. F.; Zhu, G. Y.; Vugrinovich, B.; Kataphinan, W.; Reneker, D. H.; Wang, P. *Biotechnol. Prog.* **2002**, *18*, 1027–1032.

(8) Kanwar, S. S.; Pathak, S.; Verma, H. K.; Kumar, S.; Gupta, R.; Chimni, S. S.; Chauhan, G. S. *J. Appl. Polym. Sci.* **2006**, *100*, 4636–4644.
(9) Nikolaev, A. L.; Chicherin, D. S.; Sinani, V. A.; Noa, O. V.; Melikhov, I. V.; Plate, N. A. *Polym. Sci.* **2001**, *43*, 21–25.
(10) Jia, H.; Zhu, G.; Wang, P. *Biotechnol. Bioeng.* **2003**, *84*, 406–414.
(11) Daubresse, C.; Grandfils, C.; Jerome, R.; Teyssie, P. *Colloid Polym. Sci.* **1996**, *274*, 482–489.
(12) Pinnavaia, T. J. *Science* **1983**, *220*, 365–371.
(13) Tzialla, A. A.; Pavlidis, I. V. *Bioresour. Technol.* **2010**, *101*, 1587–1594.
(14) Serefoglou, E.; Litina, K. *Chem. Mater.* **2008**, *20*, 4106–4115.
(15) Secundo, F.; Miehé-Brendlé, J.; Chelaru, C.; Ferrandi, E. E.; Dumitriu, E. *Microporous Mesoporous Mater.* **2008**, *109*, 350–371.
(16) Georgakilas, V.; Gournis, D.; Petridis, D. *Angew. Chem., Int. Ed.* **2001**, *40*, 4286–4288.
(17) Giannelis, E. P. *Adv. Mater.* **1996**, *8*, 29–35.
(18) Ohtsuka, K. *Chem. Mater.* **1997**, *9*, 2039–2050.
(19) Gopinath, S.; Sugunan, S. *Appl. Clay Sci.* **2007**, *35*, 67–75.
(20) Gopinath, S.; Sugunan, S. *Catal. Commun* **2005**, *6*, 525–530.
(21) Cristofaro, A.; De; Violante, A. *J. Colloid Interface Sci.* **2005**, *290*, 39–44.
(22) Galindo-González, C.; de Vicente, J.; Ramos-Tejada, M. M.; López-López, M. T.; González-Caballero, F.; Durán, J. D. G. *Langmuir* **2005**, *21*, 4410–4419.
(23) Oliveiraa, L. C. A.; Riosa, R. V. R. A.; Fabrisa, J. D.; Sapagb, K.; Gargc, V. K.; Lagoa, R. M. *Appl. Clay Sci.* **2003**, *22*, 169–177.
(24) Bourlinos, A. B.; Karakassides, M. A.; Simopoulos, A.; Petridis, D. *Chem. Mater.* **2000**, *12*, 2640–2645.
(25) Szabó, T.; Bakandritsos, A.; Tzitzios, V.; Papp, S.; Korösi, L.; Galbács, G.; Musabekov, K.; Bolatova, D.; Petridis, D.; Dékány, I. *Nanotechnology* **2007**, *18*, 285602–285610.
(26) Ovsejevi, K.; Grazúa, V.; Cuadraa, K.; Batista-Viera, F. *Enzyme Microb. Technol.* **2004**, *35*, 203–209.
(27) Grazú, V.; Abian, O.; Mateo, C.; Batista-Viera, F.; Fernández-Lafuente, R.; Guisán, J. M. *Biomacromolecules* **2003**, *4*, 1495–1501.
(28) Kara, A.; Osman, B.; Yavuz, H.; Beşirli, N.; Denizli, A. *React. Funct. Polym.* **2005**, *62*, 61–68.
(29) Brena, B. M.; Ryden, L.; Porath, G. J. *Biotechnol. Appl. Biochem.* **1994**, *19*, 217–231.
(30) Haupt, B.; Neumann, T.; Wittemann, A.; Ballauff, M. *Biomacromolecules* **2005**, *6*, 948–955.
(31) Arica, M. Y.; Soydogan, H.; Bayramoglu, G. *Bioprocess Biosyst. Eng.* **2010**, *33*, 227–236.
(32) Bayramoğlu, G.; Yılmaz, M.; Şenel, A. Ü.; Arıca, M. Y. *Biochem. Eng. J.* **2008**, *40*, 262–274.
(33) Alonso-Morales, N.; López-Gallego, F.; Betancor, L.; Hidalgo, A.; Mateo, C.; Fernández-Lafuente, R.; Guisán, J. M. *Biotechnol. Prog.* **2004**, *20*, 533–536.
(34) Arıca, M. Y.; Bayramoğlu, G. *J. Mol. Catal. B: Enzym.* **2004**, *27*, 255–265.
(35) Deng, H.; Li, X. L.; Peng, Q.; Wang, X.; Chen, J. P.; Li, Y. D. *Angew. Chem., Int. Ed.* **2005**, *44*, 2782–2785.
(36) Bradford, M. M. *Anal. Biochem.* **1976**, *72*, 248–254.
(37) Nelson, N. *J. Biol. Chem.* **1944**, *153*, 375–380.
(38) Miller, G. N. *Anal. Chem.* **1959**, *81*, 426–428.
(39) DeLouise, L. A.; Miller, B. L. *Anal. Chem.* **2005**, *77*, 1950–1956.
(40) Gendreau, R. M.; Burton, R. *Appl. Spectrosc.* **1979**, *33*, 581–584.
(41) Sato, H.; Ono, K.; Johnston, C. T.; Yamagishi, A. *Am. Mineral.* **2004**, *89*, 1581–1585.
(42) Janek, M.; Emmerich, K.; Heissler, S.; Nüesch, R. *Chem. Mater.* **2007**, *19*, 684–693.
(43) Deng, H.; Li, X.; Peng, Q.; Wang, X.; Chen, J.; Li, Y. *Angew. Chem., Int. Ed.* **2005**, *44*, 2782–2785.
(44) Nandwana, V.; Elkins, K. E.; Poudyal, N.; Chaubey, G. S.; Yano, K.; Liu, J. P. *J. Phys. Chem. C* **2007**, *111*, 4185–4189.
(45) Rose, M.; Bohlmann, W.; Sabo, M.; Kaskel, S. *Chem. Commun.* **2008**, *21*, 2462–2464.
(46) Li, X. G.; Feng, H.; Huang, M. R. *Chem.—Eur. J.* **2010**, *16*, 10113–10123.
(47) Bolgar, M. S.; Gaskell, S. J. *Anal. Chem.* **1996**, *68*, 2325–2330.
(48) Mohanty, A. K.; Misra, M.; Drzal, L. T. *Natural fibers, biopolymers, and biocomposites*; CRC: Boca Raton, FL, 2005; pp 704−705.
(49) Jarzębski, A. B.; Szymańska, K.; Bryjak, J.; Mrowiec-Białoń *J. Catal. Today* **2007**, *124*, 2–10.